COMPLIANT MICROTRANSMISSIONS FOR RECTILINEAR ELECTROTHERMAL ACTUATORS

Larry L. Chu, Joel A. Hetrick*, and Yogesh B. Gianchandani[1]

Department of Electrical and Computer Engineering, University of Wisconsin, Madison, USA
*Department of Mechanical Engineering, University of Wisconsin, Madison, USA

ABSTRACT

This paper reports on synthesized designs of compliant microstructures used to modify the force-displacement relationships of electrothermal actuators. The design process uses truss elements and involves topology synthesis and dimensional optimization in a two-stage approach. In order to accommodate buckling constraints, it limits the stress on beam segments. Measurements of devices fabricated from 11.5 μm thick p^{++} Si and 55 μm electroplated Ni as structural materials match theoretical predictions within 20%. Rectilinear non-resonant displacements up to 100 μm and amplification factors >20x are obtained.

Keywords: actuators, compliant mechanisms, design

I. INTRODUCTION

Compliant mechanisms are structures that deform elastically to transmit a force or displacement [1-4]. They are relatively immune to backlash and friction, and their monolithic designs are suitable for lithography-based fabrication. These aspects make them attractive for microsystems applications.

Electrothermal actuation of compliant microstructures has been used in a variety of ways [5-9]. One promising application of compliant mechanisms is in microtransmissions. In particular, they are well-suited to transform the high force and moderate displacement of electrothermal actuators into moderate force, high displacement outputs. For example, bent-beam electrothermal actuators of the type described in [6,7] provide *rectilinear* motion with peak displacement in the range of 5-30 μm and blocking force (which is defined as the force that nulls the displacement) in the range of 1-10 mN. It will be shown that microtransmissions can significantly increase the peak displacement. Past applications of microtransmissions to *rectilinear* actuators have included the use of electrostatic actuators. In [10], an electrostatic actuator offering displacements up to 20 μm was reported. However, the availability of substantially higher output forces from electrothermal actuators can permit even higher displacements to be achieved. In [11], an electrothermal actuator offering a non-resonant displacement of 20 μm was reported. In this paper, a new topology is explored for the microtransmission. It provides a geometric advantage ≈20x, resulting in ≈100 μm displacement. The use of stress constraints in the design permits this performance to be achieved with relatively thin structural material. Devices were fabricated using both p^{++} Si and electroplated Ni as structural materials. The design procedure and test results are presented in the following sections.

II. DESIGN SYNTHESIS

The design procedure is broken into topology synthesis and dimensional synthesis. Each stage is posed as a structural optimization problem, where the objective is to maximize the blocking force and/or unloaded output displacement given all relevant design constraints. The primary characteristics of the actuator are the block force, F_{block1}, (i.e. the maximum force at zero displacement) and unloaded output displacement, d_{out1}. When a compliant mechanism is coupled to an electro-thermal-compliant actuator, it can transform these two quantities to produce a new block force, F_{block2}, and unloaded output displacement, d_{out2}. Depending on the design, the compliant mechanism can achieve extreme amplification of the block force or output displacement, as required by the application. The amplification factor, A, is expressed as the ratio of the output displacement to the input (actuator) displacement:

$$A = \frac{d_{out2}}{d_{out1}} \qquad (1)$$

While amplification change is one method for determining the magnification factor, other methods such as specifying the ratio of blocking forces, or the slope change two force-displacement relationships can also be readily accommodated.

Analysis is performed using structural truss and beam elements along with linear, static finite element theory (for the moment coupled electrical and thermal effects are neglected). For both topology synthesis and dimensional synthesis, the finite element equilibrium analysis and the constrained optimization problem are solved within MATLAB™. Optimization is performed using MATLAB's Sequential Quadratic Programming (SQP) algorithm. Design derivatives are calculated using the adjoint variable method and by directly differentiating the stiffness matrix with respect to size and node position design variables.

[1]Address:1415 Engineering Drive, Madison, WI 53706-1691; Tel: (608) 262-2233, Fax: 262-1267, E-mail: yogesh@engr.wisc.edu

The generic structural optimization problem (for both topology and dimensional synthesis) is posed as follows:

$$\text{Max } F_{block2} \cdot d_{out2} - P\left(\frac{d_{out2}}{d_{out1}} - A^*\right)^2 \qquad (2)$$

$$\text{subject to:}$$

$$\sigma_{axial} - \sigma_{buckling} \le 0; \quad V - V_{allow} \le 0$$

$$h_{\min} \le h_i \le h_{\max}; \quad X_{\min} \le X_j \le X_{\max}; \quad Y_{\min} \le Y_k \le Y_{\max}$$

The required amplification factor, A^*, is enforced by penalizing the objective function by the penalty factor, P. Buckling is enforced by limiting the maximum axial stress to $\sigma_{buckling}$ based on Euler's buckling criteria, modified for end conditions (during dimensional synthesis). The total volume constraint is enforced by V_{allow}. Design variables include element width and node position co-ordinates, denoted by h_i, X_j, and Y_k respectively. During dimensional synthesis these are given local upper and lower bounds that serve to limit the search space and also enforce fabrication limitations.

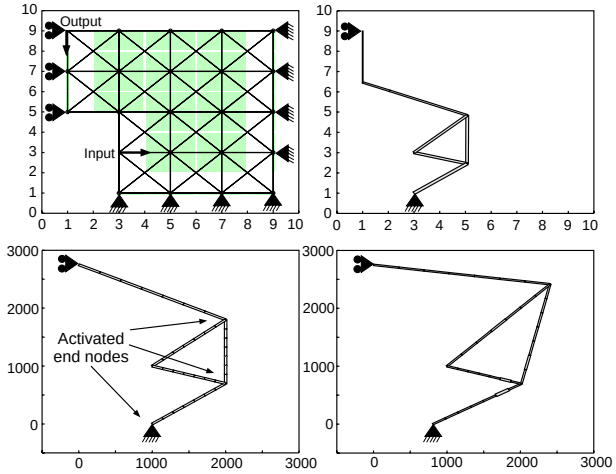

Fig. 1: Steps in the synthesis of a microtransmission. (a-upper left): Assuming symmetry, half the design domain is meshed with truss elements; (b-upper right): Optimized topology is determined; (c-lower left): Design is re-meshed for dimensional synthesis; (d-lower right): Final design obtained.

To establish the optimal topology of a mechanism, the design domain is discretized using a network of truss elements, defined as a ground structure. The topology optimization process seeks to resize each element thickness until the performance of the structure is maximized. Upon completion, elements that converge to the lower bound are removed yielding the final mechanism topology. The topology synthesis approach described here utilizes a modular ground structure where nodes are allowed to change location within 'wandering limits'. Research has shown that this technique produces good topology designs that accurately satisfy magnification requirements [12].

Since the actuators are symmetrical about the axis of motion, the microtransmissions can take advantage of symmetry, which allows only half of the topology to be designed, which lowers computational requirements. For the following example, the modulus was set to 1000, the width was set to 1, the total volume constraint was set to 2, and the lower element bound was set at 1E-4. To achieve the magnification factor of 20, the penalty multiplier was set to 1. Figure 1a shows the floating-node ground structure, discretized using 25 nodes and 72 elements; 23 nodes were activated and given wandering ranges resulting in 107 design variables (wandering ranges indicated by gray areas). Figure 1b indicates the optimal topology of the compliant mechanism amplifier with elements converging to the lower bound removed.

To proceed with dimensional synthesis, each segment of the topology is re-meshed using arrays of beam elements; the number of elements along an array is directly controlled by the designer. Exact specifications for the material modulus, out-of-plane thickness, input actuator characteristics, and desired magnification are input into the optimization routine. The designer may choose to activate end nodes of topology segments, allowing for geometric variation. Intermediate nodes along the length of an activated segment are adjusted by maintaining a collinear equidistant relationship.

Figure 1c shows the inverter example from the topology synthesis re-meshed for the secondary dimensional synthesis stage. Constraints within the fabrication sequence that pose upper or lower bonds on the various dimensions of the structural components can be defined at this point. In this example, the thickness and the minimum widths of the elements were set to 15 μm. Figure 1d shows the optimized structure (M = 20, P = 1, V_{allow} = 1x10^6 μm^3). This particular design offers a blocking force of 470 μN assuming a Young's modulus (E) of 100 GPa, and a free displacement of 51 μm. The force is proportional to E. Because of the minimum width limitation, substantial energy is spent deforming the compliant transmission (transmission efficiency is 14.1 percent). Larger blocking force and free displacement can be achieved by fabricating more flexible structures with thinner beam widths (within buckling limitations).

An example of a synthesized design is shown in Fig. 2. The entire web-like mechanism is suspended above the substrate and attached to it only at the anchors. Current is passed between the nodes V^+ and V^-. The symmetry of the design confines the current to centrally located bent beam actuators, which provide lateral input displacements to the microtransmission. This generates an axial displacement at the output node, as shown. Incorporation of stress constraints in eqn. (2) to reduce the propensity for out-of-plane buckling results in the selective widening of beams that are in

compression when actuated. In addition, the longest beam, which is attached to the output node, is in tension.

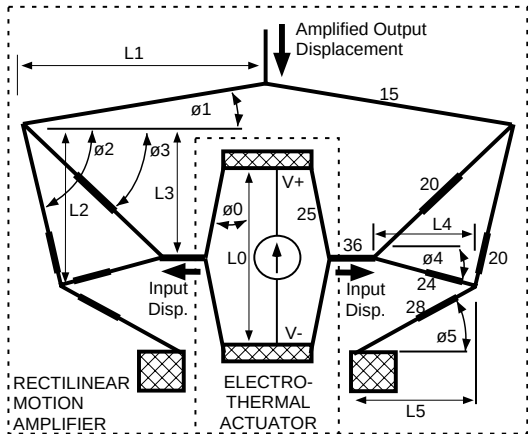

Fig. 2: A synthesized microtransmission with two bent beam actuators providing lateral input forces. Cross-hatched areas represent anchors which attach the structure to the substrate.

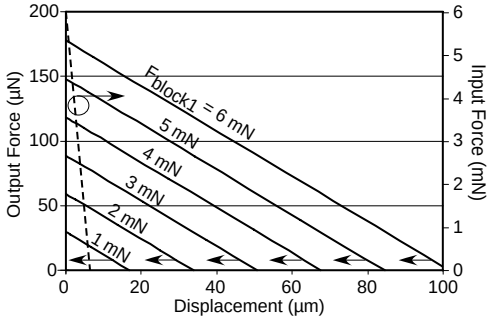

Fig. 3: Load lines for an individual bent-beam actuators and for a symmetric half of device L1 with the topology of Fig. 2 and dimensions as defined in Table I.

Table I: Dimensions of fabricated devices as defined in Fig. 2. R_w denotes ratio of actual beam widths to those indicated. Structural material was 11.5 µm thick p^{++} Si.

Dev #	L0 µm	L1 µm	L2 µm	L3 µm	L4 µm	L5 µm	R_w
L1	2450	2415	1750	1400	1000	1210	1.0
L2	2450	2180	1450	1150	985	1105	1.0
L3	1838	1182	1313	1050	750	908	0.71
S1	1225	1208	875	700	500	605	0.42

Figure 3 shows results from the finite element analysis (FEA) of a device of the type shown in Fig. 2. Since the device is laterally symmetric, only half the structure was modeled. The dimensional variables were as denoted for device L1 in Table I. Material properties reflected the use of p^{++} Si as the structural material. The thickness of the entire structure was assumed to be 11.5 µm. The figure shows the load line of an individual bent-beam actuator, along with a family of load lines at the output of the mechanism under different levels of actuation. The level of actuation, which is controlled by the electrical power applied to the bent-beams, is represented by the parameter F_{block1}. It is clear from this figure that the microtransmission converts a load line which has force and displacement axis intercepts of 6 mN and 5.8 µm, to those which have intercepts in range of 250 µN and 100 µm, respectively. It is important to note that the FEA was performed for only half the structure, and the actual output force is twice that indicated in Fig. 3. The calculated amplification factor, A_{calc}, is 17.5 for this device.

From a design perspective, it is convenient to begin with the target force and displacement required at the output of the mechanism. If A and M are known for the selected transmission, the force and displacement required at its input can be calculated. The bent-beam actuator can then be designed using the analytical equations for its unloaded displacement (d_{out1}) and maximum force (F_{block1}) described in [7]. It must be able to provide the force and displacement required by the transmission without buckling.

III. EXPERIMENTAL RESULTS

Mechanisms were fabricated from both p^{++} Si and electroplated Ni to demonstrate the operation of the microtransmissions. The p^{++} Si devices were 11.5 µm thick, and were fabricated on glass wafers by the dissolved wafer process [13]. A sample device is shown in Fig. 4a. The dimensional parameters of fabricated designs are listed in Table I. A current was passed through the electro-thermal actuators and the displacements were measured at both the input and output of the microtransmission. The measurements were taken by a calibrated visual method, with an uncertainty of <0.5 µm. The results are summarized in Table II, along with calculated performance. For example, device L1 achieved 100.4 µm output displacement when driven by 105 mA of current, and the measured amplification factor, A_{meas}, was 17.0. This compares very well with the predicted value of 17.5. The detailed response of this device is shown in Fig. 5. Its best use appears to be at output displacements below 90 µm for which the input power is about 650 mW. Device L3, achieved 86.2 µm output displacement when driven by 85 mA current. Its A_{meas} of 21.4 was higher than predicted possibly because the a portion of the suspension may have been heated.

Electroplated Ni samples were fabricated using the LIGA process [14]. These devices were 55 µm thick and were fabricated on a glass substrate as well. A 2 µm thick Cu sacrificial layer also served as the base for electroplating. For the electroplating conditions used, E=115±10 GPa [15]. A sample device is shown in Fig. 4b. In this design, the microtransmission was driven by two pairs of bent-beam actuators at each lateral input. A non-resonant displacement of 85 µm was measured at an input of 0.9V. For this device, A_{calc}=8.2, and A_{meas}=9.3.

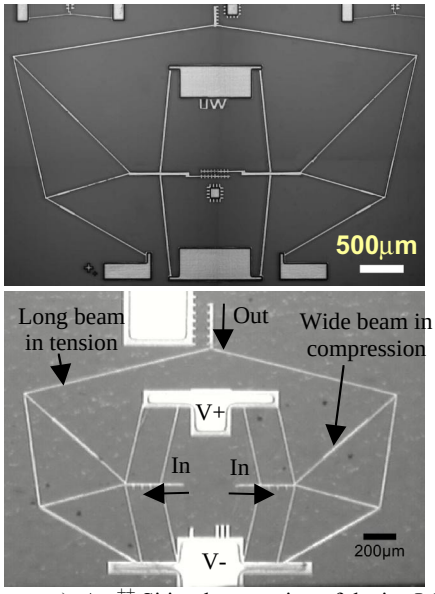

Fig. 4: (a-upper): A p^{++} Si implementation of device L1; (b-lower) A Ni implementation of a similar design.

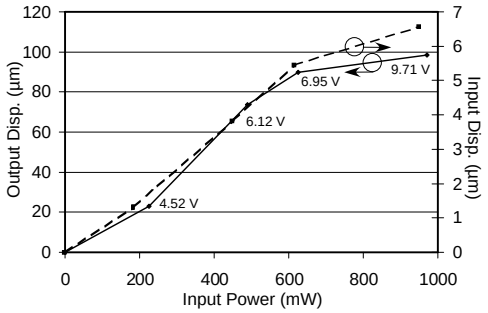

Fig. 5: Measured displacement at the input (d_{out1}) and output (d_{out2}) of the microtransmission for device L1.

Table II: Summary of simulated and measured results. Calculations assume p^{++} Si structural material, uniform ΔT=500°C, 3 ppm/K expansion coeff., and E=180 GPa.

		Calculated			Measured	
Dev. #	I mA	d_{out2} μm	F_{block2} μN	A_{calc}	A_{meas}	d_{out2} μm
L1	105	102	178	17.5	17.0	100.4
L2	90	57.1	514	9.1	8.6	34.1
L3	86.2			17.5	21.4	85.0
S1	47.6	53.6	64.0	17.6	18.6	55.0

IV. CONCLUSIONS

Compliant microtransmissions that provide amplification factors >20x when driven by electrothermal actuators have been demonstrated. The designs were synthesized using truss elements. The two-stage process included topology synthesis followed by the dimensional optimization. In order to reduce the propensity of out-of-plane buckling, stress constraints were used in addition to dimensional and volume limits.

The devices were fabricated using both electroplated Ni and p^{++} Si. Measurements confirmed that the multiplication factor was within 20% of the calculated estimate. Non-resonant displacements up to 100 μm were achieved. Higher performance is expected for devices with larger thickness-to-beam width ratios.

ACKNOWLEDGEMENTS

This effort was supported in part by NSF grant #9985422 to author YBG.

REFERENCES

[1] G. Ananthasuresh, S. Kota, N. Kikuchi, "Strategies for Systematic Synthesis of Compliant MEMS," *Dynamic Systems and Control,* DSC-v. 55-2, ASME Winter Annual Meeting, Chicago, Nov. 1994, pp. 677-86

[2] O. Sigmund, "Tailoring Materials with Prescribed Elastic Properties," *Mechanics of Materials,* v. 20, '95, pp. 351-68

[3] S. Nishiwaki, M. Frecker, M. Seungjae, N. Kikuchi, "Topology Optimization of Compliant Mechanisms Using the Homogenization Method,", *Intl. J. Numerical Methods in Engineering,* 42(3), 1998, pp. 535-559

[4] S. Kota, J. Hetrick, Z. Li, L. Saggere, "Tailoring Unconventional actuators using compliant transmissions: Design Methods and Applications," *IEEE Trans. on Mechatronics,* 4(4), 1999, pp. 396-408

[5] H. Guckel, J. Klein, T. Christenson, K. Skrobis, M. Laudon, E. Lovell, "Thermo-Magnetic Metal Flexure Actuators," *Solid-State Sensor & Actuator Workshop,* Hilton Head, SC, June 1992, pp. 73-75

[6] L. Que, J.-S. Park, Y.B. Gianchandani, "Bent-Beam Electro-Thermal Actuators for High Force Applications," *IEEE Intl. Conf. on MEMS,* Orlando, Florida, Jan. 1999

[7] J.-S. Park, L.L Chu, E. Siwapornsathain, A.D. Oliver, Y.B. Gianchandani, "Long Throw and Rotary Output Electro-Thermal Actuators Based on Bent-Beam Suspensions," *IEEE Intl. Conf. on MEMS,* Miyazaki, Japan, Jan. 2000

[8] J.Jonsmann, O.Sigmund, S.Bouwstra, "Compliant Thermal Microactuators," *Sensors & Actuators,* v. 76, 1999, pp. 463-9

[9] T. Moulton, G. Ananthasuresh, "Micromechanical Devices with Embedded Electro-Thermal-Compliant Actuation," *MEMS-Vol. 1,* ASME International Mechanical Engineering Conference and Exposition, MEMS, Nov. 1999, Nashville, Tenessee, pp. 553-560

[10] S. Kota, J. Hetrick, Z. Li, S. Rodgers, T. Krygowski, "Synthesizing High-Performance Compliant Stroke Amplification Systems for MEMS," *IEEE Intl. Conf. On MEMS,* Miyazaki, Japan, Jan. 2000

[11] L. Chu, J. Hetrick, Y. Gianchandani, "Electro-Thermal Actuators Using Optimized Compliant MicroTransmissions as Rectilinear Motion Amplifiers, *Solid-State Sensors & Actuators Workshop,* Hilton Head, S.C., June 2000

[12] J. Hetrick, *A Unified Approach for Topological and Dimensional Synthesis of Compliant Mechanisms,* Ph.D. Thesis, Univ. of Michigan, Ann Arbor, Michigan, 1999

[13] Y. Gianchandani, K. Najafi, "A Bulk Silicon Dissolved Wafer Process for Microelectromechanical Systems," *IEEE J. of Microelectromechanical Systems,* 1(2), 1992, pp. 77-85

[14] H. Guckel, "High-Aspect-Ratio Micromachining Via Deep X-Ray Lithography," *Proc. IEEE,* 86(8), '98, pp.1586-93

[15] L. Chu, L. Que, Y. Gianchandani, "Temperature Coefficients of Material Properties for Electrodeposited MEMS," *IEEE Intl. Conf. on MEMS,* Interlaken, Jan. 2001